Supplementary Information

I Movie Captions

Movie 1: Fluid like dynamics of virus rods within the cyclic polygon membrane assembled from fdY21M-PEG and M13KO7Y21M mixture imaged using simultaneous phrase contrast and fluorescence microscopy, where 1 in 30,000 long rods (M13KO7Y21M) are fluorescently labeled. Therefore, individual rods pointing out of the screen appear as bright green spots. The rods freely diffuse within the membrane. Scale bar, 5 μm.

Movie 2: Lateral coalescence of a fdY21M-PEG membrane (smaller in size/ on right) with a M13KO7Y21M membrane (larger in size/ on left) at dextran 52 mg/ml imaged using DIC microscopy. Two small aggregates of "defective rods" (highlighted by two arrows) present along the M13KO7Y21M membrane edge move swiftly towards each other under capillary flow of fdY21M-PEG rods. Eventually, these two aggregates come very close to each to other and form a junction diametrically opposite to the location of initial contact between two membranes. Scale bar, 10 μm.

Movie 3: Lateral coalescence of a fdY21M-PEG membrane (smaller in size) with a M13KO7Y21M membrane (larger in size) where edges of both the membranes are macroscopically clean, at Dextran 52 mg/ml imaged using DIC microscopy. This movie clearly provides evidence for presence of optically non-resolvable defective rods that accumulate under capillary flow of fdY21M-PEG rods to form a macroscopically large pinning junction highlighted by an arrow in the movie. Scale bar, 10 μm.

Movie 4: Lateral coalescence of a fdY21M-PEG membrane (smaller in size) with a M13KO7Y21M membrane (larger in size) at dextran 52 mg/ml imaged using 2D LC-PolScope microscopy. Membrane edges show significant PolScope signal indicating edge bound rods are tilted with respect to membrane normal with a finite twist penetration depth. Flow of fdY21M-PEG rods along the edge of the M13KO7Y21M membrane results in development of an interface separating two kinds of rods with barely detectable PolScope signal. This implies that edge bound M13KO7Y21M rods untwist to be part of the liquid membrane core and the rods that fail to do so are carried by the fdY21M-PEG rods capillary flow to form the pinning junction. Scale bar, 10 μm.

Movie 5: Lateral coalescence of fdY21M-PEG (on right, smaller in size) with a M13KO7Y21M membrane (on left, larger in size) is co-imaged using phase contrast and fluorescence microscopy. Both membranes are largely composed of non-fluorescent rods. However, M13KO7Y21M membrane is sparsely doped with fluorescently labeled M13KO7Y21M rods (ratio of number of labeled to unlabeled rods is about 5:10,000). Edge bound rods lie nearly completely in the imaging plane and appear as short bright line segments in fluorescence microscopy. Two big open arrows indicate the flow of edge bound M13KO7Y21M rods from two opposite directions as the fdY2M-PEG rods spread over the M13KO7Y21M membrane edge. Among these edge bound bright rods, one rod indicated by a filled arrow flows like any other edge bound rod but failed to untwist (time stamp 00:45 to 01:43) and eventually becomes part of the pinning junction. Scale bar, 10 μm.

Movie 6: Simultaneous bright-field and fluorescence imaging of lateral coalescence of a fdY21M-PEG membrane (smaller in size, bright fluorescent) with a M13KO7Y21M membrane (larger in size) having a major fraction of its edge covered with macroscopic clumps of defective rods. Here, only fdY21M-PEG rods are fluorescently labeled. Presence of large number of defective rods halts the spread of fdY21M-PEG rods to less than 50% perimeter of the M13KO7Y21M membrane edge and thus, results in a pinning line after the completion of coalescence. Scale bar, 10 μm.

Movie 7: Lateral coalescence of resultant membrane from Movie 2 with a M13KO7Y21M membrane (on right) which shows formation of second pinning junction, at dextran 52 mg/ml imaged using DIC microscopy. During the event, two large islands of M13KO7Y21M rods connected to each pinning junction coalesce in plane to form single liquid core. Thus, such sequential coalescence events give rise to a faceted liquid core of long rods (M13KO7Y21M) and overall shapes the membrane into cyclic polygon like geometry. Scale bar, 10 μm.

Movie 8: Dynamics of the M13KO7Y21M rods at the pinning junction where 1 in 10,000 M13KO7Y21M rods are fluorescently labeled in cyclic polygon like colloidal membrane. One of the fluorescently labeled rod is seen to be temporarily stuck (encircled in movie) at the pinning junction which gets dislodged at 10:52. Scale bar, 5 μm.

Movie 9: Lateral coalescence of a large fdY21M-PEG membrane (fluorescent) with a small M13KO7Y21M membrane at dextran 52 mg/ml, imaged using DIC and fluorescence microscopy alternately. Similar to other coales-

cence movies, here too pinning junction is formed but pinches off at later stage. Detachment of M13KO7Y21M circular island from membrane edge is clearly visible in fluorescence where the host fdY21M-PEG membrane appears bright. (Time stamp - 08:36 and after 34:51). Scale bar, 10 μm.

II Is pinning junction a topological defect?

Typically topological defects are formed either through discontinuity in inclinations, that is, disclination or discontinuity in location, that is, dislocation. Screw and edge dislocations in Smectic A phase stem from the lattice structure posed by the layering. However, since colloidal membranes are effectively monolayer smectic A like phase, dislocations are not commonly observed in this system [1]. In fact, all the defects observed in colloidal membranes so far are disclinations [2, 3].

We image the fdY21M-PEG, M13K07Y21M and one junction composite membranes using 2D-LC-PolScope microscopy to establish the possibility of pinning junctions to be a topological defect. We perform PolScope microscopy with normal incidence of imaging light on the membrane plane (x-y) as well as imaging light incident at an angle with respect to x-z plane (Fig. S5a,b)[3]. The normal and angled illumination for this technique are henceforth referred to as regular and titled PolScope imaging. These two modes of imaging enable us to experimentally determine handedness of rod tilts in the membrane edge. Pixel intensity in a PolScope image is directly proportional to the local tilt of the rods with respect to the direction of illuminating light (z - axis) which is same as the membrane normal in case of regular PolScope. Thus we find uniform PolScope signal along the membrane edge with a finite twist penetration depth indicating edge bound rods are significantly tilted with respect to membrane normal (Fig. S5a,c,e). In fact, the rods at the periphery of the membrane edge lie completely in the plane of imaging [4].

We slightly off-center the illuminating light source from conventional alignment along z-axis with a almost closed aperture such that the light source illuminates the membrane plane (x-y) at an angle with respect to x-z plane in the tilted Polscope set-up. With this arrangement, the edge bound rods that are tilted towards the direction of illuminating light will result in lesser optical retardance whereas for the rods that tilt away form direction of illumination will result in higher optical restardance. Membrane images recorded in this arrangement of tilted PolScope are shown in Fig. S5b,d,f

where left region of the membrane edges (indicated by white arrows) are less brighter than right region (indicated by red arrows). We quantify the difference in retardance of the membranes imaged in regular and tilted PolScope setup by plotting it (Fig. S5g-l) along the direction shown by dashed line with arrow head (inset of Fig. S5g-l) which is along off-center direction of light source. In case of regular PolScope, the two retardance peaks corresponding to diametrically opposite portions of a membrane edge show nearly equal values of peak retardance for all the membranes (Fig. S5g,i,k)). We set the location of first peak to zero of position axis, Fig. S5g-l. In the contrast, the retardance peaks associated with same portions of respective membrane edge attain unequal peak retardnace values in the tilted PolScope (Fig. S5h,j,l). We observe decrease in peak retardance of first peak for both fdY21M-PEG and M13KO7Y21M membranes in tilted PolScope (Fig. S5h,j). This implies that both membranes have same handedness. The outermost edge of the one junction composite membrane is majorly fdY21M-PEG rods and thus without surprise shows similar trend of decrease in peak retardance values. As mentioned in the main text, the PolScope image of one junction composite membrane shows barely detectable signal from two rod interface (Fig. S5k,l). So we zoom into retardance plot of Fig. S5k,l from position = 0.8 μm to 27 μm (inset plot Fig. S5k,l) to understand the microscopic tilts of rods at the interface. The inset plot of Fig. S5k shows two distinct peaks at 1.3 μm and 25 μm associated with the two rod interface within one junction composite membrane in regular PolScope microscopy. The first peak around 1.3 μm becomes nearly negligible and the second peak at 25 μm gets slightly enhanced in the tilted PolScope microscopy of the same two rod interface. We conclude from this information that handedness of the two rod interface in the one junction composite membrane is in the same direction as its outermost membrane edge or membranes assembled from fdY21M-PEG/M13K07Y21M virus rods.

We now represent the tilts/handedness of M13KO7Y21M and fdY21M-PEG membranes prior to, during and post coalescence process schematically in Fig. S6 a-c (indicated by arrows) based on the experimental data discussed above. 180°or π radians of twist is trapped in the region of coalescence which results in the formation of pore like defects that are evident in the early parts of the Movie 5 (time stamp 00:00 to 00:05) [2]. However, this defect is annealed completely by flipping/rotation of fdY21M-PEG membrane under thermal fluctuations once most of this membrane has spread over the larger M13KO7Y21M membrane (time stamp 01:44 to 05:40). This results in a composite membrane which schematically appears as shown in Fig. S6 (b). There are three locations in this composite membrane, marked as A, B and C, where one may consider the possibility of disclination. No discontinuity

in inclination exists in the outermost region of A and B because both type of rods have the same direction of handedness. The inner interface marked as C also tilts in the same direction as the outermost rod-polymer interface in the one junction membrane as shown in Fig. S5e,f,k,l. Notably, the retardance, proportional to local tilt of the rods, of the interface C is ten times smaller than outermost membrane edge. These imply that there are two possibilities regarding the microscopic nature of the interface C. First, one of the rods could twist in a direction opposite to its natural preferred direction to maintain continuity in the tilt as one goes across this interface. This will, of course, be energetically expensive. Second, since the interface has little to no twist associated with it, shorter rods could remain untwisted with the longer rods twisting in their preferred natural direction to match up at the boundary. Regardless of the microscopic nature of the interface C, the fact that its handedness is the same as the regions surrounding A and B avoids discontinuity in inclination throughout the one-junction membrane schematically shown in Fig. S6 (c). Therefore, we conclude that the pinning junctions reported in this work are likely to be not topological defects.

III Supplementary Figures

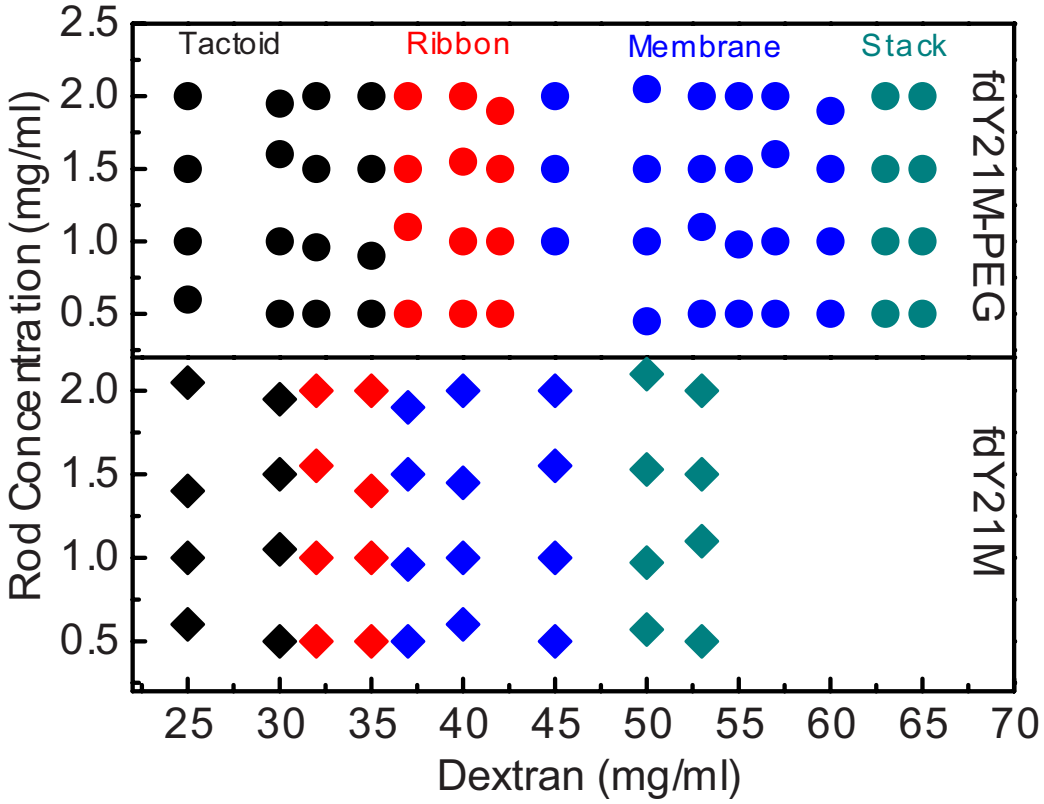

Figure S1. Phase diagram of fdY21M-PEG and fdY21M. Comparison of phase diagram of PEG coated fdY21M to bare fdY21M virus as a function of rod concentration and depletant (dextran) concentration. fdY21M-PEG phase diagram shifts towards higher dextran concentration as compared to that required for the bare viruses. This is due to steric repulsion between PEG molecules that needs to be overcome by addition of more dextran.

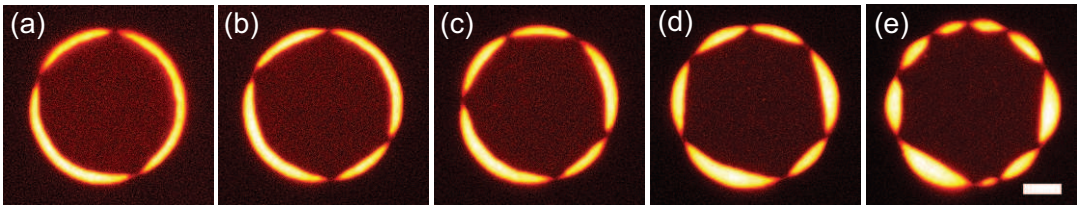

Figure S2. Cyclic polygon like colloidal membranes with sequentially increasing number of pinning junctions ($\mathbf{N}_p$). (a) $N_p = 3$, (b) $N_p = 4$, (c) $N_p = 5$, (d) $N_p = 6$ and (e) $N_p = 9$. Scale bar, 5 μm

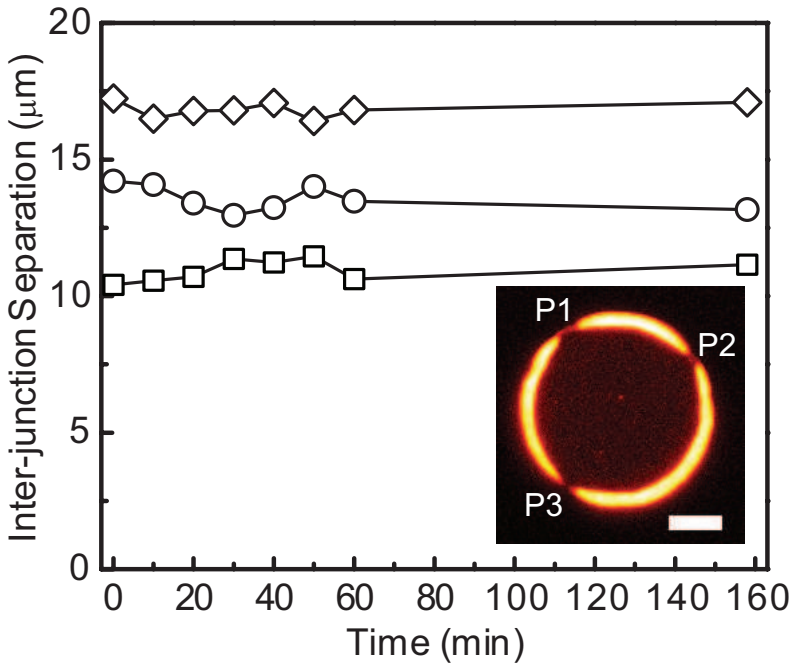

Figure S3. Variation of inter-junction separation with time. P1, P2 and P3 are pinning junctions of cyclic polygon like colloidal membrane shown in the inset. Scale bar, 5 μm. Open circles, open squares and open diamonds show separation between P1-P3, P1-P2 and P2-P3, respectively. Inter-junction separation nearly remains constant for a well equilibrated membrane.

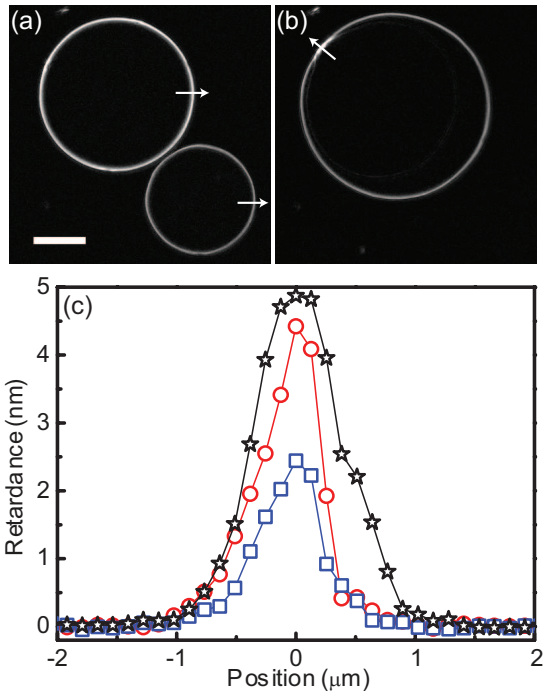

Figure S4. Retardance of membranes imaged using 2D LC-PolScope microscopy. PolScope images of (a) membranes composed of purely M13KO7Y21M rods (larger membrane), purely fdY21M-PEG rods (smaller membrane), and (b) one junction composite membrane formed after completion of coalescence of the membranes shown in (a). Scale bar, 10 μm. Each pixel intensity value is directly proportional to the local retardance at that point. (c) Retardance line profile along arrows indicated in (a-b) for purely M13KO7Y21M membrane edge (open red circles), purely fdY21M-PEG membrane edge (open blue squares) and over the pinning junction of the composite membrane (open black stars). Retardance line profile over the pinning junction has maximum retardance value of 4.87 nm compared to the corresponding values for the individual membranes of fdY21M-PEG (2.5 nm) or M13KO7Y21M (4.4 nm). This larger PolScope signal associated with the pinning junction arises because the signal is also dependent on layer thickness which increases locally due to accumulation of defective rods into a point or a line in our case.

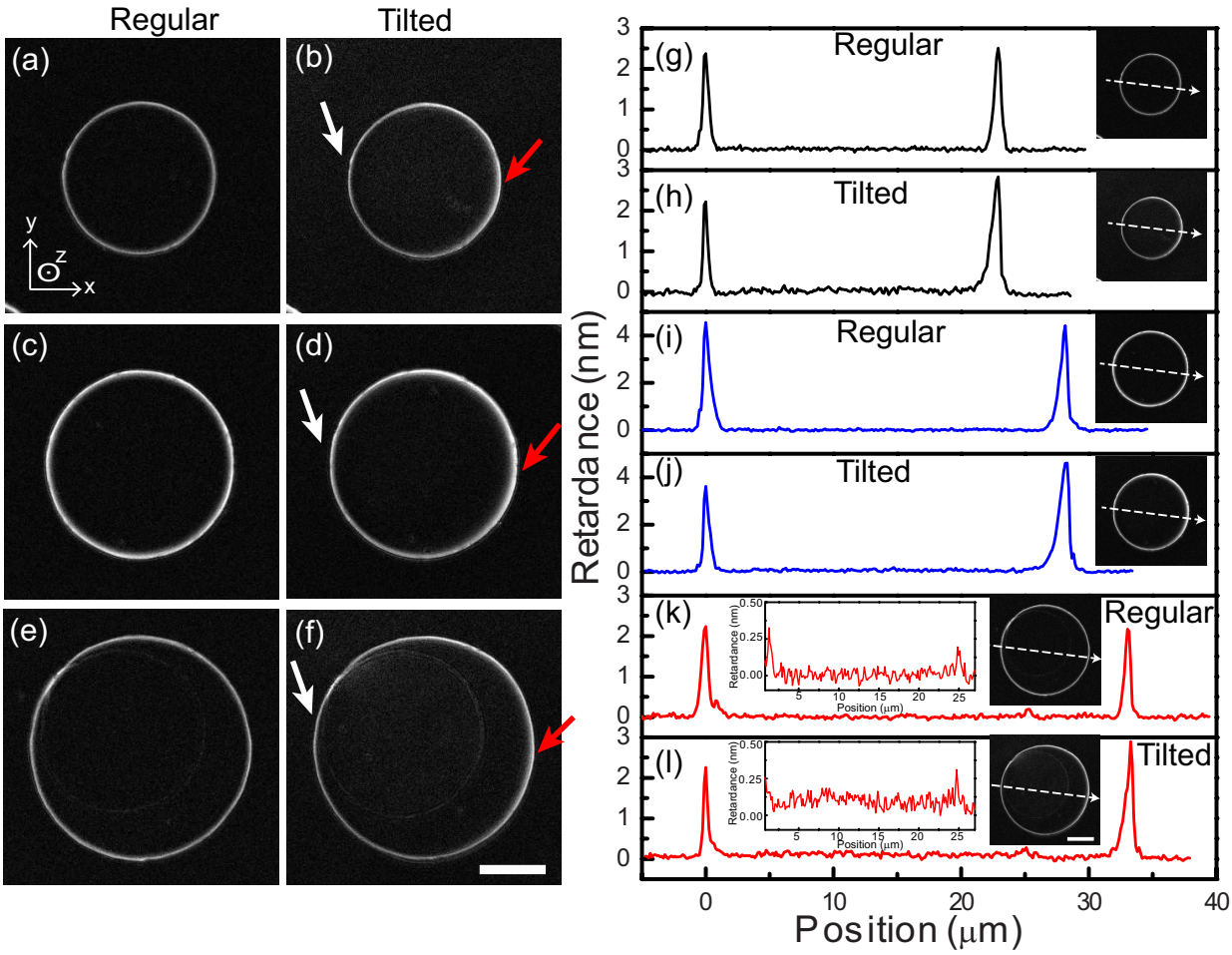

Figure S5. 2D-LC-PolScope images and their respective retardance plot. Regular 2D-LC-PolScope images of (a) fdY21M-PEG, (c) M13KO7Y21M and (e) one junction composite membrane where imaging light illuminates the membrane plane (x-y) at normal incidence. (b), (d) and (f) are corresponding tilted 2D-LC-PolScope image of membranes in (a),(c) and (e) respectively where membrane plane is illuminated at an angled incidence. (g)-(l) membrane retardance plotted along the white dash line with arrow head shown in respective insets (black - fdY21M-PEG, blue - M13K07Y21M and red - one junction composite membrane). The inset plot of (k) and (l) are zoomed part of its respective plot from position = 0.8 μm to 27 μm. Scale bar, 10 μm.

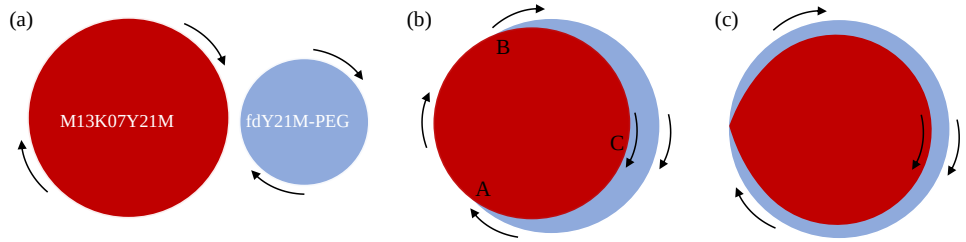

Figure S6. Schematic comparing respective tilts/handedness of membranes. Direction of arrows represent the tilts/handedness of edge bound rods in respective membranes (a) prior to, (b) during and (c) post coalescence process. The possible locations for appearance of any topological defect are denoted by A, B and interface C in (b). As no conflict of rod tilt arises at these locations, shown by arrows in (b) and (c), we rule out possibility of pinning junction to be any topological defect.

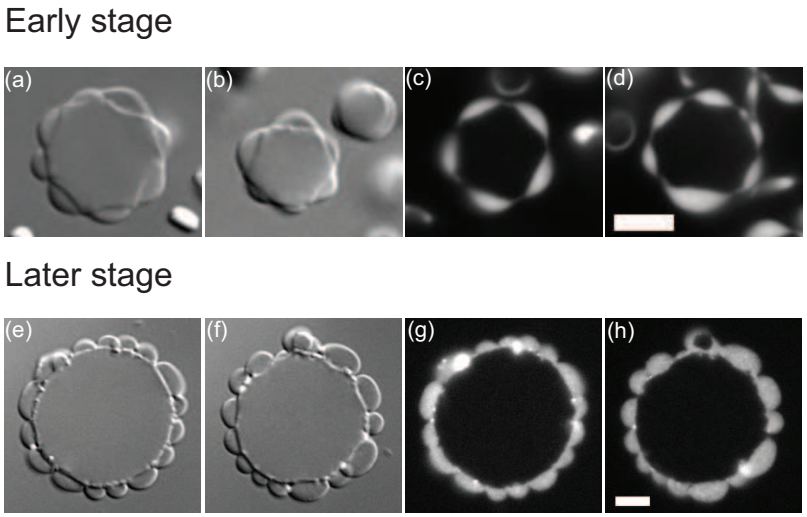

Figure S7. Colloidal membranes assembled from M13KO7Y21M (70%) and fd-PEG (30%) mixture at dextran 57 mg/ml. (a)-(b) DIC images of colloidal membrane assembled from M13KO7Y21M and fd-PEG mixture within two hours of sample preparation where in-plane protruding lobes are predominantly fd-PEG rods, resembling cyclic polygon membranes. (c)-(d) Similar membranes imaged using fluorescence microscopy where fd-PEG rods are fluorescently labeled and thus lobes appear bright. (e)-(f)

DIC images of well equilibrated colloidal membranes of M13KO7Y21M and fd-PEG mixture observed after thirty hours of sample preparation. (g)-(h) Similar membranes imaged using fluorescence microscopy where fd-PEG rods are fluorescently labeled. These images show that the equilibrium shape of membranes assembled from oppositely chiral rods was that of a garland surrounding the circular inner core instead of the initial cyclic polygon shape. Scale bar, 5 μm.

References

[1] C. Nadir Kaplan and Robert B. Meyer. Colloidal membranes of hard rods: unified theory of free edge structure and twist walls. *Soft Matter*, 10:4700–4710, 2014.

[2] Mark J. Zakhary, Thomas Gibaud, C. Nadir Kaplan, Edward Barry, Rudolf Oldenbourg, Robert B. Meyer, and Zvonimir Dogic. Imprintable membranes from incomplete chiral coalescence. *Nature Communications*, 5:3063, Jan 2014. Article.

[3] Thomas Gibaud, C. Nadir Kaplan, Prerna Sharma, Mark J. Zakhary, Andrew Ward, Rudolf Oldenbourg, Robert B. Meyer, Randall D. Kamien, Thomas R. Powers, and Zvonimir Dogic. Achiral symmetry breaking and positive gaussian modulus lead to scalloped colloidal membranes. *Proceedings of the National Academy of Sciences*, 114(17):E3376–E3384, 2017.

[4] Edward Barry, Zvonimir Dogic, Robert B. Meyer, Robert A. Pelcovits, and Rudolf Oldenbourg. Direct measurement of the twist penetration length in a single smectic a layer of colloidal virus particles. *The Journal of Physical Chemistry B*, 113(12):3910–3913, Mar 2009.